

## COHERENT STRUCTURES AND THEIR CONTRIBUTION TO TURBULENT INTENSITY IN TURBULENT CHANNEL FLOW

**Shintaro Imayama**

Department of Energy Engineering and Science,  
Nagoya University,  
Furo-cho, Chikusa-ku, Nagoya, 464-8603, Japan  
imayama.shintaro@f.mbox.nagoya-u.ac.jp

**Yoshinobu Yamamoto**

Department of Nuclear Engineering,  
Kyoto University  
Yoshida, Sakyo, Kyoto, 606-8503, Japan  
yyama@nucleng.kyoto-u.ac.jp

**Yoshiyuki Tsuji**

Department of Energy Engineering and Science,  
Nagoya University,  
Furo-cho, Chikusa-ku, Nagoya, 464-8603, Japan  
c42406a@nucc.cc.nagoya-u.ac.jp

### ABSTRACT

The measurement of stream-wise turbulent intensity normalized by inner variables is discussed in this paper. The stream-wise turbulent intensity  $u_{rms}$  normalized by friction velocity  $u_\tau$ , which is expressed as  $u_{rms}^+$ , is well known to increase with Reynolds number. Especially the trend of peak of  $u_{rms}^+$  as a function of Reynolds number has been investigated so far by many researchers. In order to clarify the  $u_{rms}^+$  profile, there are two important issues. One is the accurate velocity measurement. This is discussed from the point of hot-wire resolution. The other is the evaluation of skin friction. We have modified the classical oil-film technique and discuss its accuracy. Experimental results are compared with those of Direct Numerical Simulation (DNS).

### INTRODUCTION

Stream-wise turbulence intensity  $u_{rms}$  is a fundamental statistic in a shear flow. When it is normalized by friction velocity  $u_\tau$ ,  $u_{rms}^+ \equiv u_{rms}/u_\tau$  varies against the distance from the wall and takes its maximum around  $y^+ \simeq 15$ . It is known that the inner-scaled peak in the stream-wise turbulent intensity,  $(u_{rms}^+)_{peak}$ , increases with Reynolds number. For instance, the typical example is seen in the papers; Hutchins & Marusic (2007), DeGraaf & Eaton (2000) and Metzger & Klewicki (2001). In Hutchins & Marusic (2007), they compared many experimental and DNS data, and suggested the empirical fitting curve;

$$(u_{rms}^+)_{peak} = \sqrt{1.036 + 0.965 \ln(Re_\tau)}, \quad (1)$$

which is available up to  $Re_\tau \simeq 10^6$ . Here, the Reynolds number is defined by  $Re_\tau = u_\tau \delta / \nu$ .  $\delta$  is a boundary layer thickness or the half channel height. Equation 1 is obtained by a least square fitting of many available data. However, the collected data scatter around the fitting curve. There is also small discrepancy between experiments and DNS. Where is this discrepancy coming from? Is it an experimen-

tal error? In this paper we try to reply these questions and would like to emphasize how difficult to measure accurately the normalized turbulence intensity is.

### EXPERIMENTAL CONDITIONS

The measurements are performed in a channel as sketched in Fig. 1. The cross-sectional area is  $W = 650$  mm in width and  $H = 50$  mm in height, and therefore an aspect ratio is  $W/H = 13$ . This ratio is enough large to avoid the effect of flow developed from the side wall. The total channel length is 10400 mm. Transition into turbulence is promoted by DYMO tape set up at the channel entrance. Both the shear stress and velocity profile are measured at a distance of  $164H$  from the channel inlet. This length is sufficient to get a fully developed turbulent flow before reaching the measuring section. We used the ordinary hot-wire operated by constant temperature anemometry and the oil film interferometry technique. These are briefly explained in the following.

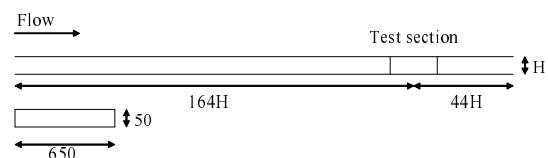


Figure 1: Schematic view of channel flow setup.

### Oil Film Interferometry

A small size of oil drops on the wall of channel test section. When the flow blows, the oil is then extended by the imposed wall shear stress at the free surface and changes its shape to enough thin oil film. The oil film illuminated by a sodium lamp (the wave length:  $\lambda = 589$  nm) begins to show a fringe pattern. The fringe velocity  $u_k$  is calcu-

lated by the succeeding images of fringe pattern. The wall shear stress is obtained by assigning the fringe velocity into Eq.(2), which is derived from Navier-Stokes equation and mass balance (Naughton&Sheplak,2002):

$$\tau_0 = \mu u_k \frac{2 n^2 - \sin^2 \alpha}{\lambda [k + h_0/h]}^{1/2} \quad (2)$$

where subscript  $k$  indicates the  $k$ th black fringe pattern.  $h_0$  is the height of the first black fringe at the film edge, and  $h$  is the height difference between two consecutive fringes:

$$h = \frac{\lambda}{2 n^2 - \sin^2 \alpha}^{1/2} \quad (3)$$

where  $n$  is the refractive index of oil, and  $\alpha$  is the camera viewing angle as shown in Fig. 2. A clear image of fringe pattern is necessary to evaluate the skin friction accurately. An anti-reflection coating lens is set at the top wall, which is located between the camera lens and the oil. The reflection of the part which is reflected by replaced anti-reflection coating lens is suppressed, and the high contrast and sharp image is obtained (see Fig. 3).

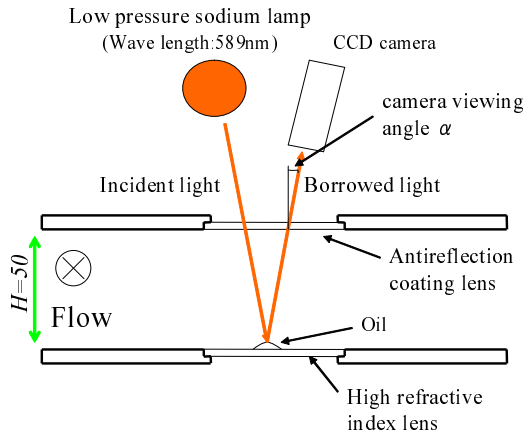


Figure 2: Oil film interferometry setup. The flow direction is from heads to tails.

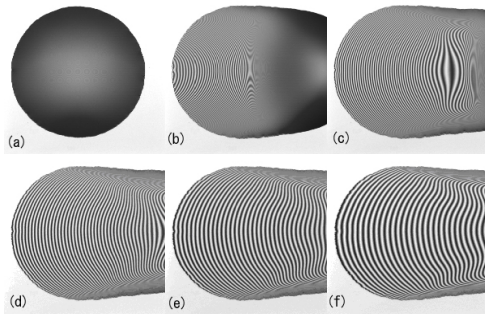


Figure 3: Typical examples of oil film fringe patterns. Flow direction is from left to right. (a)  $t=0$ sec, (b)  $t=100$ sec, (c)  $t=200$ sec, (d)  $t=300$ sec, (e)  $t=400$ sec, (f)  $t=500$ sec

Measured skin friction coefficients are plotted together with DNS value in Fig.4. Although we have used two different viscosity oils, they present the similar trends and matched with DNS sufficiently. The solid line indicates the least square fitting curve;  $c_f = 0.611 Re_m^{-0.254}$ , where  $Re_m$  is the Reynolds number defined by  $Re_m = U_m H/2$ , and  $U_m$  is the cross-sectional averaged velocity. It is found that

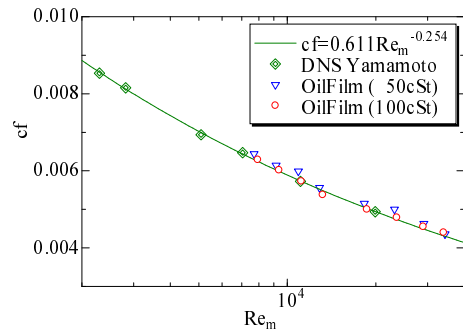


Figure 4: Local skin friction coefficient measured in present experiment and DNS.

present experiments and DNS matched with each other within  $\pm 2\%$ .

**Velocity Measurement**

I-type probe, operated by a house-made constant temperature anemometer (CTA) with overheat ratio 0.5, is used for velocity measurement. The sensitive area is made of tungsten, whose diameter is  $5 \mu m$  and  $0.74 mm$  in length. The signal from CTA is digitized in a personal computer using a 16 bit A/D converter at a sampling frequency of 20 kHz and sampling period of 60 sec. Velocity is measured at the same position with that of oil film measurement.

**DIRECT NUMERICAL SIMULATION**

The continuity and incompressive Navier-Stokes equations were computed by a hybrid spectral and finite difference method (Yamamoto et. al., 2008). Fourier spectral method was used as the stream and spanwise spatial discretization method and nonlinear terms were computed with 1.5 times finer grids to remove aliasing errors. The wall-normal derivatives were solved by a second-order finite difference scheme at staggered grid arrangements. Time integration method was low-storage 3rd-order Runge-Kutta scheme for convection terms, Crank-Nicolson scheme for viscous terms and Euler Implicit scheme for Pressure terms, respectively. Streamwise mean pressure gradient was imposed as the driving force and non-slip at the walls and periodic conditions for stream and spanwise directions were adapted for boundary conditions. In case of  $Re_\tau = 1000$  used 768, 1032 and 768 grids in stream, wall-normal and spanwise directions, respectively, the computational time per one step was about 90 sec on Fujitsu HPC2500/256CPUs at Information Technology Center, Nagoya University. Present DNS accuracies were verified compared with results of delAlamo and Jimenez, 2003 as shown in Fig.5.

**RESULTS AND DISCUSSIONS**

Mean velocity profile is plotted in Fig. 6 together with DNS. The vertical and horizontal axes are normalized by inner variables, and the Reynolds number is set at  $Re_\tau \approx 1000$ . Present experiment matches DNS completely. And other Reynolds numbers are in Fig. 7. The solid line represents log law;  $U^+ = 1/\kappa \ln y^+ + B$  with Karmen constant  $\kappa = 0.41$  and additive constant is 5.0. It is hard to find out the log-law region at this Reynolds number, but it is noted that the solid line is slightly smaller than the present results. The normalized turbulent intensity is plotted in Fig. 8. There

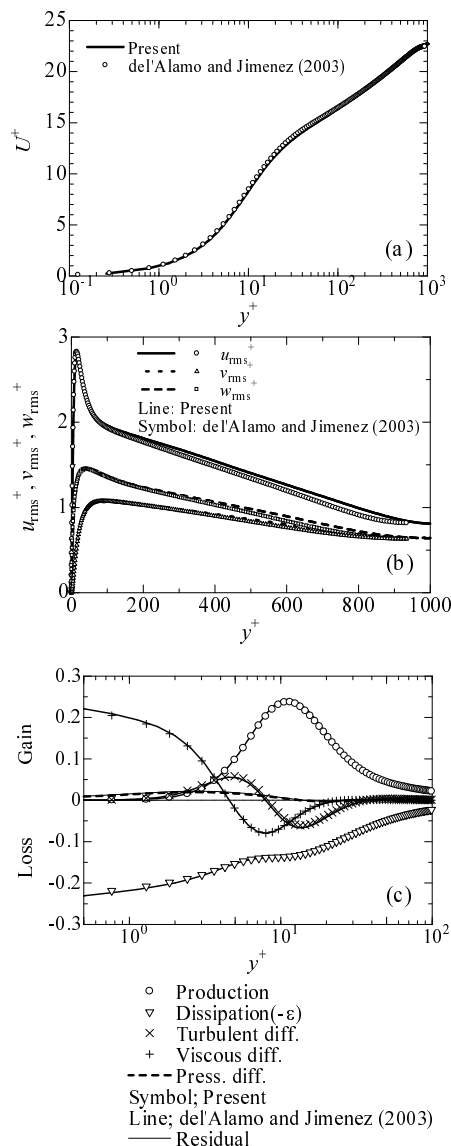


Figure 5: Verifications of the present DNS accuracy compared with results of deAlamo and Jimenez(2003); (a)Mean velocity, (b)Turbulent intensities, (c)Turbulent kinetic energy budget,  $Re_\tau = 1000$ .

is a large deviation between experiment and DNS. Although the gap is small in the outer region, it becomes much larger in inner region. The peak value  $(u_{rms}^+)_{peak}$  significantly decreases. We assume this difference might be attributed to the spanwise spatial resolution of hotwire. When the sensitive length  $\ell$  is normalized by friction velocity,  $\ell^+ = u_\tau \ell / \nu$  is 29.8 for the case of  $Re_\tau \approx 1000$ . On the other hand in DNS, the space resolution corresponds to the grid size in span-wise direction  $z$ , which is normalized by  $u_\tau$ , and  $\ell^+ = u_\tau z / \nu$  is 4.4. Thus much higher resolution is expected in DNS.

A characteristic structure in shear flow near the wall is a streak which is shown in Fig. 9. At  $y^+ = 15$ , each streak locates in a distance of 100 wall units in span wise direction. The streaks meander in span wise direction, then if the span-wise spatial resolution of sensitive area is not enough, the small scale fluctuations are averaged over the sensitive area. This makes the peak  $(u_{rms}^+)_{peak}$  attenuate significantly. This observation can be checked by analyzing the DNS data. Instantaneous streamwise velocity is averaged

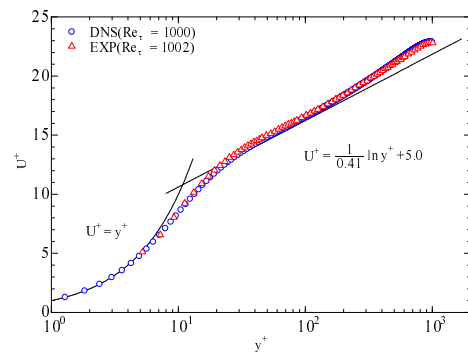


Figure 6: Mean velocity profile compared the hotwire to DNS.

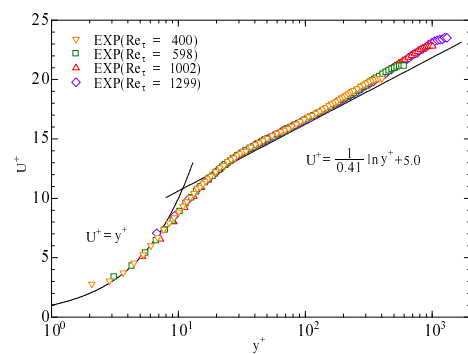


Figure 7: Mean velocity profiles for  $400 < Re_\tau < 1299$ .

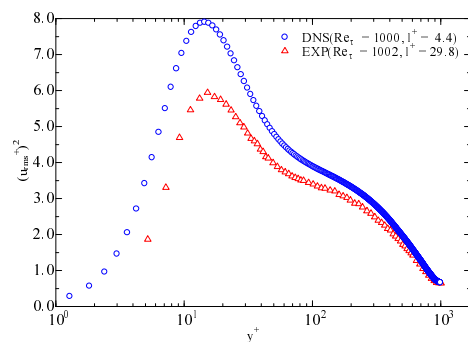


Figure 8: Turbulence intensities profile compared hot wire to DNS.

over some length in spanwise direction and the root mean square is calculated. The averaged area corresponds to the spatial resolution of hotwire. The results are plotted in Fig. 10. It is noted that  $(u_{rms}^+)_{peak}$  decreases as the spatial resolution becomes poor. In the outer region, the attenuation is small but not zero. It is because the small scale motion still survives even at the channel centerline.  $(u_{rms}^+)_{peak}$  is plotted as a function of  $\ell^+$  in Fig. 11. The peak value asymptotically increases for small  $\ell^+$ . It is expected to have a finite value for  $\ell^+ \rightarrow 0$ . This simple analysis teaches us that  $(u_{rms}^+)_{peak}$  is not only a function of Reynolds number but also a function of spatial resolution.

The difference between experiment and DNS in the inner region, which is larger than outer region, becomes clear in the contour of pre-multiplied spectrum. One-dimensional energy spectrum of stream-wise velocity fluctuation is defined as  $E(k)$ , where  $k$  is the wave number of streamwise

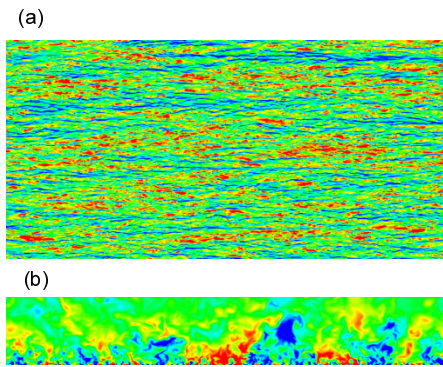


Figure 9: Instant velocity fluctuation calculated by DNS for  $Re_\tau = 1000$ . (a) x-z plane at  $y^+ = 15$ , (b) y-z plane.

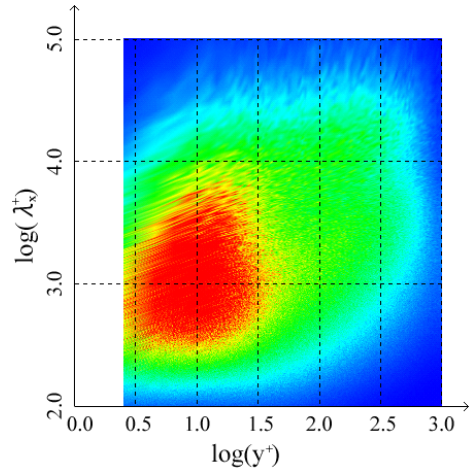


Figure 12: 1-D pre-multiplied spectra of streamwise velocity fluctuation measured by using hot wire for  $Re_\tau \approx 1000$ .  $0(blue) < kE(k)/u_\tau^2 < 4(red)$ .

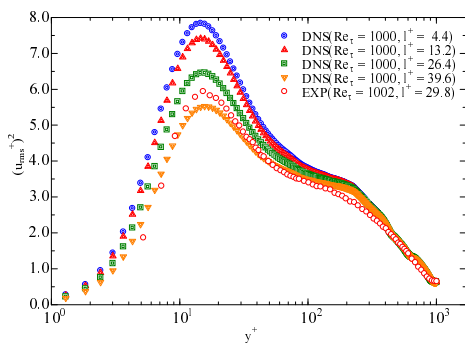


Figure 10: Turbulence intensities profile for different spatial resolution. Experiment and DNS.

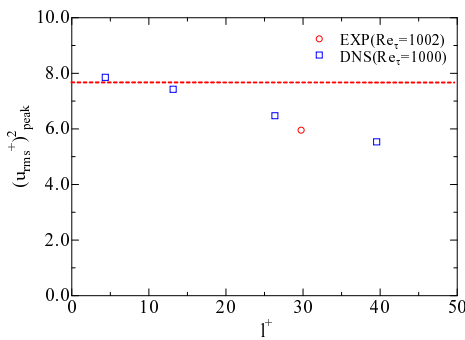


Figure 11:  $(u_{rms}^+)^2_{peak}$  is plotted as a function of spatial resolution  $l^+$ . Dashed line is Eq. (1).

direction calculated by Taylor's hypothesis. The one-dimensional pre-multiplied spectrum is calculated as  $kE(k)$ . The contour map of pre-multiplied spectra normalized by the friction velocity with wall normal position is shown in Fig. 12. The vertical axis is the stream-wise wavelength normalized by the friction velocity and kinematic viscosity. From the contour of pre-multiplied spectrum, it is shown that the fluctuation is caused by both small and large scale structures in inner region, but in outer region, fluctuation is mainly caused by large scales. That is, the difference observed in Fig. 8 is understood as follows, the small scale fluctuations become large in inner region, but such motions are not possible to be detected by the poor span-wise special resolution. It is clearly seen in Fig. 12 that PMS can not resolve small scales  $\log \lambda^+ < 2.2$ . This is the main reason of attenuating the turbulent intensity near the wall. In the outer region,

large scale fluctuation is well measured by the present probe size, then the difference between experiment and DNS is small.

It is also interesting to study the turbulent intensity profile in boundary layer, and it is compared with that of channel flow. Recently, much attention has been paid to the large scale motions in shear flows (boundary layer, channel flow, pipe flow). Kim & Adrian (1999) found that stream-wise energetic modes can be extended up to 12-14 pipe radii, and refer to these as Very Large-Scale Motions (VLSM). They suggested that VLSM may be agglomeration of hairpin packets. Hutchins & Marusic (2007) named these as "super-structure(SS)". SS exists in the log and lower wake regions of turbulent boundary layers. We assume that SS plays an important role to contribute the turbulent intensity. But it is not clearly understood, because the normalized turbulent intensity is strongly affected by the friction velocity. To evaluate accurately the turbulence intensities in the inner region and outer region, it is important to measure both the friction velocity and turbulence intensities. We would like to comment on this point in the presentation.

REFERENCES

K. Kim and R. J. Adrian, 1999, Physics of Fluids, vol.11,pp.417-422.  
 N. Hutchins and I. Marusic, 2007, J.Fluid Mech., vol.579, pp.1-28.  
 D.B.DeGraa and J.K.Eaton, 2000, J.Fluid Mech., vol.422,pp.319-346.  
 M.M.Metzger and J.C.Klewicky, 2001, Phys. of Fluids, vol.13,pp.692-701.  
 Jonathan W. Naughton, Mark Sheplak, 2002, Progress in Aerospace Sciences, vol.38,pp.515-570.  
 Y.Yamamoto, T. Kunugi, S.Satake and S. Smolentsev, 2008, J. Fusion Eng. and Design. vol.83, pp.1309-1312.  
 J.C.del Álamo and J. Jim énez, 2003, Phys. Fluids vol. 15, L41.